Stem Cell Reports
Article

OPEN ACCESS

A *PITX3*-EGFP Reporter Line Reveals Connectivity of Dopamine and Non-dopamine Neuronal Subtypes in Grafts Generated from Human Embryonic Stem Cells

Jonathan C. Niclis,[1] Carlos W. Gantner,[1] Cameron P.J. Hunt,[1,2] Jessica A. Kauhausen,[1] Jennifer C. Durnall,[1] John M. Haynes,[2] Colin W. Pouton,[2] Clare L. Parish,[1,3,*] and Lachlan H. Thompson[1,3,*]
[1]Florey Institute of Neuroscience and Mental Health, Royal Parade, Parkville, VIC 3010, Australia
[2]Monash Institute of Pharmaceutical Sciences, Monash University, 381 Royal Parade, Parkville, VIC 3052, Australia
[3]Co-senior author
*Correspondence: cparish@unimelb.edu.au (C.L.P.), lachlant@unimelb.edu.au (L.H.T.)
http://dx.doi.org/10.1016/j.stemcr.2017.08.002

SUMMARY

Development of safe and effective stem cell-based therapies for brain repair requires an in-depth understanding of the *in vivo* properties of neural grafts generated from human stem cells. Replacing dopamine neurons in Parkinson's disease remains one of the most anticipated applications. Here, we have used a human *PITX3*-EGFP embryonic stem cell line to characterize the connectivity of stem cell-derived midbrain dopamine neurons in the dopamine-depleted host brain with an unprecedented level of specificity. The results show that the major A9 and A10 subclasses of implanted dopamine neurons innervate multiple, developmentally appropriate host targets but also that the majority of graft-derived connectivity is non-dopaminergic. These findings highlight the promise of stem cell-based procedures for anatomically correct reconstruction of specific neuronal pathways but also emphasize the scope for further refinement in order to limit the inclusion of uncharacterized and potentially unwanted cell types.

INTRODUCTION

Human pluripotent stem cells (PSCs) are a promising source of transplantable neural progenitors for cell-replacement therapies to treat neurological conditions. One of the most anticipated applications is in Parkinson's disease (PD), where proof of principle for efficacy has already been established in clinical trials using fetal midbrain grafts (Hagell and Brundin, 2001; Lindvall and Hagell, 2000). Although these trials have been problematic due to variability in clinical outcome, more than 30 years of basic and clinical research has led to refinement of the approach, and identification of important criteria for establishment of stem cells as an alternative and potentially superior donor source (Barker et al., 2015; Thompson and Bjorklund, 2012), for example the requirement that the implanted dopamine (DA) neurons establish a functional terminal network with appropriate targets in the host brain.

Detailed characterizations of fetal graft composition and structural integration have been fundamentally important for understanding graft-host connectivity and the relationship to functional outcome. Early xenografting studies using species-specific antibodies to identify fiber outgrowth from human or porcine fetal midbrain grafts placed homotopically into rat midbrain provided some of the first evidence that grafted neurons retained an intrinsic capacity for target-directed outgrowth, even in the adult host (Isacson et al., 1995; Wictorin et al., 1992). The development of transgenic reporter mice lead to more precise characterization of fiber outgrowth, including the first demonstrations of connectivity on a neuronal-subtype-specific basis (for review see Thompson and Bjorklund, 2009). Grafting of fetal midbrain from TH-GFP (Sawamoto et al., 2001) or *Pitx3*-EGFP (Zhao et al., 2004) mice allowed for precise identification of graft-derived (GFP^+) DA fiber patterns, even in the presence of residual host DA fibers, and showed that implanted DA neurons not only innervated the host striatum but also innervated appropriate extra-striatal targets, including the cortex, amygdala, and septum (Thompson et al., 2005). These studies also showed that the major A9 and A10 DA neuronal subclasses maintained developmentally appropriate target preference, innervating striatum and frontal cortex, respectively, and importantly that A9-specific innervation of dorsolateral striatum was required for restoration of motor function (Grealish et al., 2010).

The first histological characterizations of neural grafts generated from human stem cells were limited to identification of the graft core using antibodies specific for a human nuclear antigen (Brederlau et al., 2006; Cho et al., 2008; Park et al., 2005; Sonntag et al., 2007; Yang et al., 2008). Recently however, more sophisticated approaches using human stem cell lines ubiquitously expressing fluorescent reporters (Denham et al., 2012b; Doerr et al., 2017; Espuny-Camacho et al., 2013; Lu et al., 2014; Niclis et al., 2017a; Qi et al., 2017; Steinbeck et al., 2012) and human-specific antibodies against cell-surface proteins, such as polysialated nuclear cell adhesion molecule (NCAM) (Grealish et al., 2014; Kirkeby et al., 2017; Kriks et al., 2011; Sundberg et al., 2013), have dramatically improved our understanding of the capacity of stem cell-derived

grafts to integrate within the host CNS. These studies have shown that grafted neurons, generated from either embryonic stem cells (ESCs) or induced pluripotent stem cells (iPSCs), are capable of extensive axonal growth over long distances, particularly via host white matter tracts (Grealish et al., 2014; Kriks et al., 2011; Sundberg et al., 2013). However, it has thus far not been possible to characterize the specificity of these outgrowth patterns on the basis of neuronal phenotype.

Here we report that not only are grafted neurons generated from stem cells capable of long-distance innervation of host nuclei, but also that they have the capacity to do so with neuronal subtype specificity. Using a human ESC reporter line in which EGFP expression is driven by the endogenous *PITX3* promoter (*PITX3*-EGFP) allowed us to selectively identify DA-specific patterns of growth and connectivity. The results reveal the extent and specificity of dopaminergic innervation from ventral midbrain grafts generated from human PSCs. The DA neurons innervate developmentally appropriate A9 and A10 target structures with remarkable specificity, but represent only a minority of total graft outgrowth, which is largely non-dopaminergic and extends widely throughout the host brain.

RESULTS

Ventral Midbrain Differentiation of a Human PITX3-EGFP ESC Line

Here we used a reporter line with monoallelic insertion of EGFP into exon 1 of the *PITX3* gene so that both EGFP and PITX3 were driven by *PITX3* regulatory elements (Figure 1A). To generate ventral midbrain progenitors, we used the now widely favored approach (Denham et al., 2012a; Kirkeby et al., 2012; Kriks et al., 2011; Niclis et al., 2017b) that employs early signaling to instruct regional identity in parallel with neural induction (Figure 1B). As we have recently reported in detail under fully defined, xeno-free conditions (Niclis et al., 2017b), this results in rapid and efficient neural (NESTIN$^+$) specification of ventral midbrain (FOXA2$^+$/OTX2$^+$) progenitors as shown after 11 days *in vitro* (DIV) and acquisition of midbrain DA identity evident at the time of transplantation (19 DIV; Figure 1C).

Function and Composition of Human PITX3-EGFP Grafts

The experimental design is illustrated in Figure 2A, showing the timeline of rotational testing and the small subsets of animals taken for histology over the course of 7 months. The first group for histology at 4 weeks was to confirm successful engraftment, and single animals were taken at 10 and 18 weeks as a result of unrelated skin and respiratory complications. Rotational response to D-amphetamine showed that the grafts significantly reversed asymmetry previously induced by unilateral removal of the host midbrain DA neurons (Figure 2B). This was evident by 16 weeks and sustained up until the experimental endpoint at 28 weeks. Histological analysis showed a progressive, graft-specific, EGFP$^+$ innervation of the host striatum by human DA neurons (Figure 2C). At 4 and 10 weeks, prior to significant change in rotational scores, few EGFP$^+$ fibers were detected outside the immediate vicinity of the graft. At 18 weeks, dense areas of terminally ramified EGFP$^+$ fiber networks could be observed, and this expanded to cover larger areas of the host striatum by 28 weeks. The grafts grew significantly in size from 0.8 ± 0.28 mm^3 at 4 weeks (n = 4) to 7.04 ± 0.91 mm^3 by 28 weeks (n = 10; Student's t test, $p < 0.01$). The number of GFP$^+$ DA neurons, however, did not expand over this time frame: 6,081 ± 659 at 4 weeks compared with 5,268 ± 654 at 28 weeks (Student's t test, $p = 0.49$).

Immunohistological analysis showed EGFP$^+$ to be a robust indicator of DA neuronal identity *in vivo* with the vast majority (86.5%) of EGFP$^+$ cells also identified as tyrosine hydroxylase positive (TH$^+$) (Figure 3A). Grafted DA neurons also expressed mature markers indicative of the capacity to store and release dopamine, including both the vesicular monoamine transporter (VMAT2) and the dopamine transporter (DAT; Figure 3B). The EGFP$^+$ neurons were clearly heterogeneous in nature and could be distinguished based on features representative of both the major A9 and A10 classes of midbrain DA neurons. This included smaller diameter (~15–20 μm), spherical neurons consistent with A10 morphology (Figures 3C and 3H) and also larger (~20–50 μm), pyramidal neurons typical of A9 phenotype (Figures 3D and 3H). Labeling for GIRK2 and CALBINDIN also showed a mix of DA subtypes (Figures 3E–3H). Large, GIRK2$^+$ DA neurons that did not express CALBINDIN were often found in clusters near the edge of the grafts, while CALBINDIN$^+$ DA subtypes were found throughout the grafts. Cell counting showed that the fractional contribution of distinct EGFP$^+$ DA phenotypes based on expression of GIRK2 or CALBINDIN was: 46.8% ± 8.1% GIRK2$^+$/CALBINDIN$^-$, 20.8% ± 1.1% GIRK2$^+$/CALBINDIN$^+$, and 5.0% ± 1.6% GIRK2$^-$/CALBINDIN$^+$ (Figure 3I). A remaining 27.4% ± 5.7% of EGFP$^+$ cells did not express either GIRK2 or CALBINDIN.

Human Stem Cell-Derived DA Neurons Specifically Innervate Appropriate Host Targets

Dark-field imaging of chromogen-labeled immunohistochemistry for EGFP revealed a remarkably specific pattern of axonal outgrowth by the grafted DA neurons (Figure 4). Within the host striatum, EGFP$^+$ fibers formed a dense fiber network covering large areas of the head of the striatum (Figures 4A and 4D). The EGFP$^+$ fibers also extended long distances to innervate extra-striatal areas. A notable

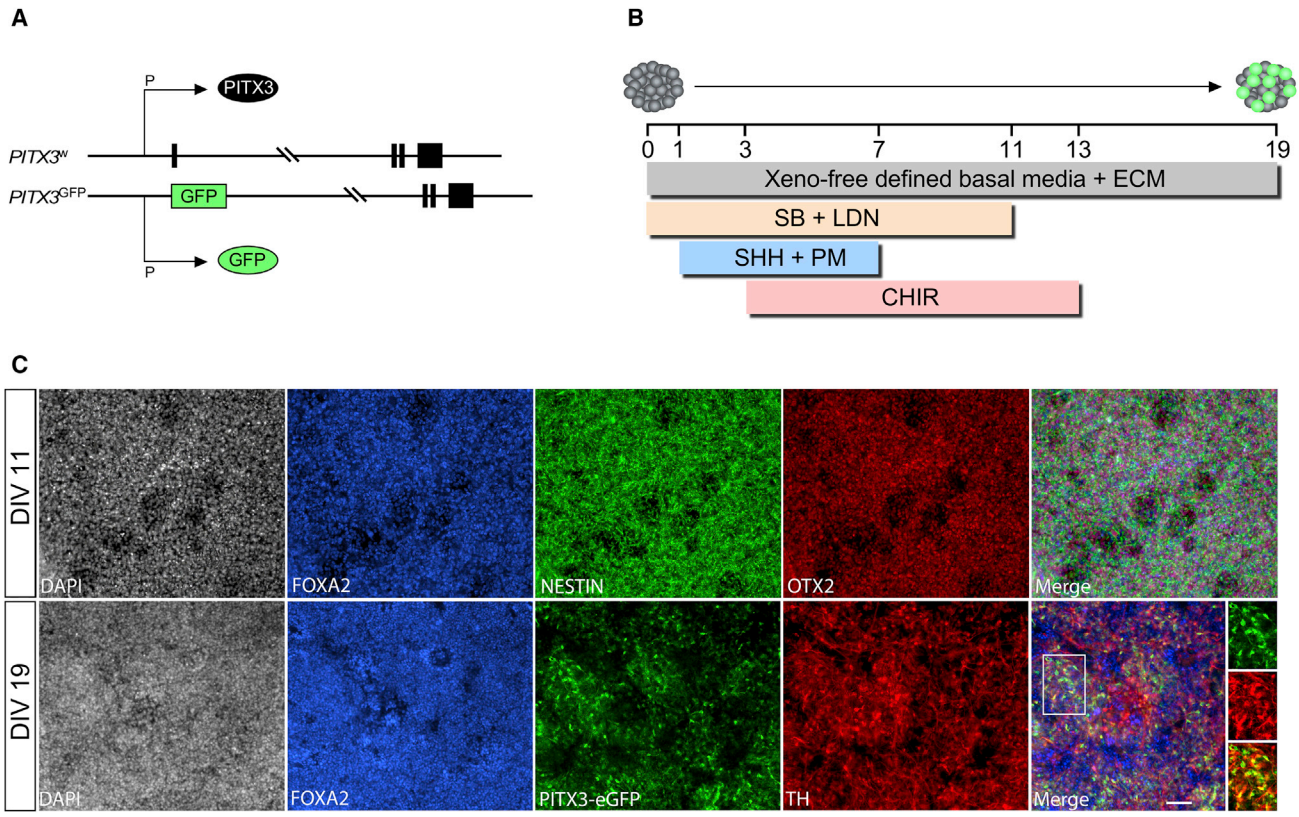

Figure 1. A Human PITX3-eGFP ES Reporter Line for Identification of Midbrain DA Neurons

(A) Monoallelic insertion of EGFP into exon 1 of the *PITX3* gene in the H9 human embryonic stem cell line to act as a reporter for PITX3 protein expression.

(B) Schematic illustration of the differentiation procedure for specification of neural progenitors with ventral midbrain identity under defined, xeno-free conditions.

(C) Differentiating cells show robust expression of markers consistent with neural (NESTIN$^+$) and ventral midbrain/forebrain (FOXA2$^+$/OTX2$^+$) identity by 11 DIV and begin to show expression of PITX3-driven EGFP and TH at the time of transplantation (19 DIV). Scale bar, 50 μm. CHIR, CHIR99021; DIV, days *in vitro*; ECM, extracellular matrix; LDN, LDN193189; PM, purmorphamine; SB, SB431542; SHH, sonic hedgehog; TH, tyrosine hydroxylase.

example included prominent growth along white matter tracts, coursing anterior to the graft through forceps minor to provide a robust innervation of the frontal cortex in a layer-specific pattern, and also the cingulate cortex directly overlying the graft (Figures 4A and 4B). A smaller innervation of the frontal cortex in the contralateral hemisphere via fibers projecting through the corpus callosum was also observed in some animals (Figure 4C). Other structures with distinct EGFP$^+$ innervation included the perirhinal cortex (Figure 4E) and the islands of Calleja through the ventral pallidum and septum (Figures 4F and 4G).

Retrograde Tracing Reveals Neuronal Subtype Specificity for Axonal Outgrowth Patterns

To characterize the neuronal identity of graft-derived innervation of distinct host target areas, we microinjected Fluorogold (FG) into either the dorsolateral striatum (Figures 5A and 5B) or frontal cortex (Figures 5C and 5D) in separate groups of animals. The deposits of FG were verified as being discretely contained within the intended target sites and clearly separated from the graft itself (Figures 5A and 5C). Across 4 animals where FG was injected into the dorsolateral striatum, 79 FG$^+$ cells were identified within the grafts and the majority of these (54; ~68%) were EGFP$^+$ DA neurons. These neurons appeared as predominately A9 in phenotype with 45 of 54 (~83%) presenting as GIRK2$^+$/CALBINDIN$^-$ and a relatively large average diameter of 35.49 μm, while a smaller fraction of cells (9 of 54) presented as either GIRK2$^-$/CALBINDIN$^+$ or GIRK2$^+$/CALBINDIN$^+$ with a smaller average diameter of 20 μm (Figures 5B and 5E).

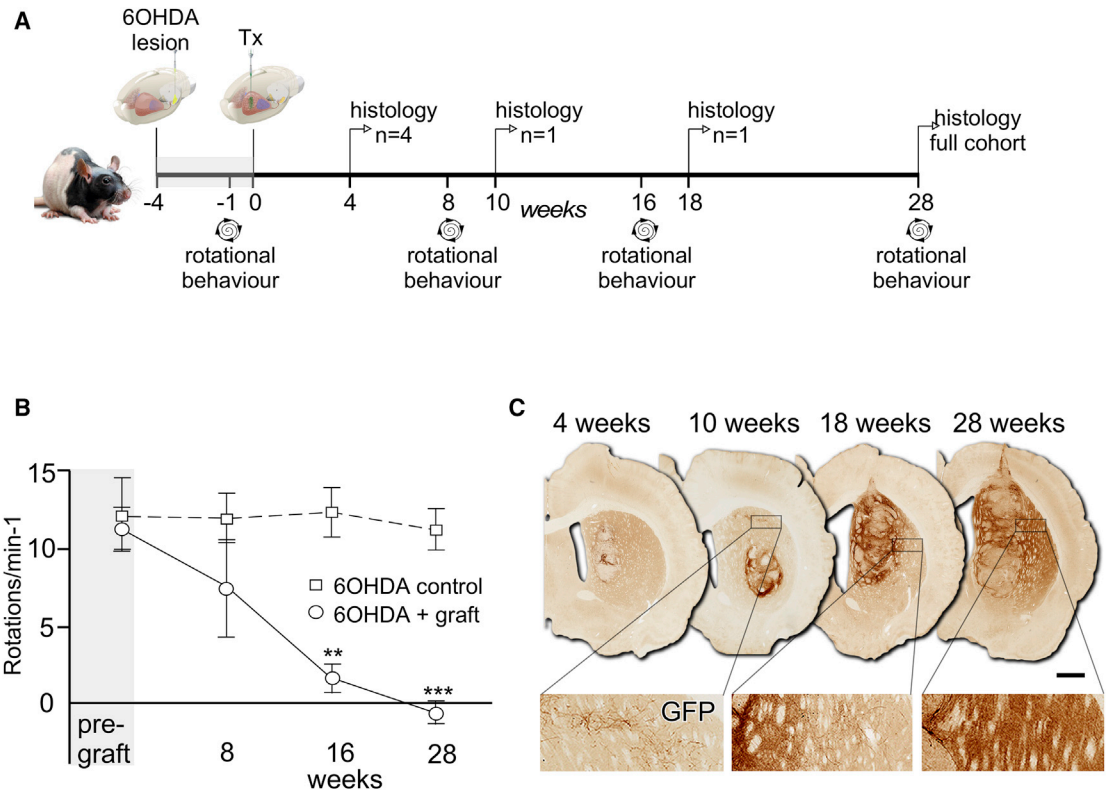

Figure 2. PITX3-eGFP Grafts Progressively Innervate the Host and Correct Motor Function

(A) Schematic illustrating experimental design and timeline. Tx, transplantation.

(B) Animals with unilateral 6-OHDA lesions showed strong rotational asymmetry in response to 2.5 mg/kg (intraperitoneal) D-amphetamine that was significantly reduced in the group (mean ± SEM) that received transplants by 16 weeks and maintained at 28 weeks (Student's t test; n = 7 for control, n = 6 for grafted; **p < 0.01, ***p < 0.005).

(C) Immunohistochemistry for EGFP in representative examples of grafted animals at 4, 10, 18, and 28 weeks showed the progressive innervation of host striatum over 6 months. Scale bar, 1 mm.

Retrograde uptake of FG from the frontal cortex identified a markedly different pattern of FG^+ cells, with the vast majority across 3 animals having a non-DA identity (93/105; ~89%). The 12 $FG^+/EGFP^+$ DA neurons were mixed in phenotype with respect to typical A9/A10 attributes. A total of 5 were $GIRK2^+/CALBINDIN^-$ and variable in size with an average diameter of 32.8 μm; while the remaining 7 expressed CALBINDIN—either alone or with GIRK2—and were notably smaller, with an average diameter of 21.86 μm (Figures 5D and 5E). Regardless of the FG injection site, larger cells with A9 features tended to reside toward the periphery of the graft, while the smaller, CALBINDIN-expressing fraction was distributed closer to the center (Figure 5E). A number of the non-DA neurons innervating the cortex co-expressed γ-aminobutyric acid (GABA) (Figure 5F), although the dense GABA immunoreactivity of the surrounding neuropil made it difficult to unambiguously quantify the proportion of FG^+ cells.

Non-dopaminergic Neurons in Stem Cell-Derived Ventral Midbrain Grafts Show Extensive Patterns of Connectivity in the Host Brain

Immunohistochemistry for EGFP and NeuN showed that the majority of differentiated neurons in the grafts were non-dopaminergic ($EGFP^-/NeuN^+$; Figure 6A). Many of these had a ventral identity, based on labeling for FOXA2, with examples also of $NeuN^-/FOXA2^+$ cells, particularly in central parts of the grafts, which may represent relatively immature ventralized progenitors. In terms of neurotransmitter phenotype, the grafts were highly immunoreactive for GABA (Figure 6B). The labeling pattern for GABA made it difficult to reliably identify $GABA^+$ cell bodies, precluding quantification; however, some cases of clearly $GABA^+$ neuronal profiles could be seen intermingled with grafted DA neurons (Figure 6C). We were not able to identify serotonin-, acetylcholine-, or noradrenaline-containing neurons.

Detection of human-specific NCAM allowed for identification of the entirety of graft-derived fiber outgrowth

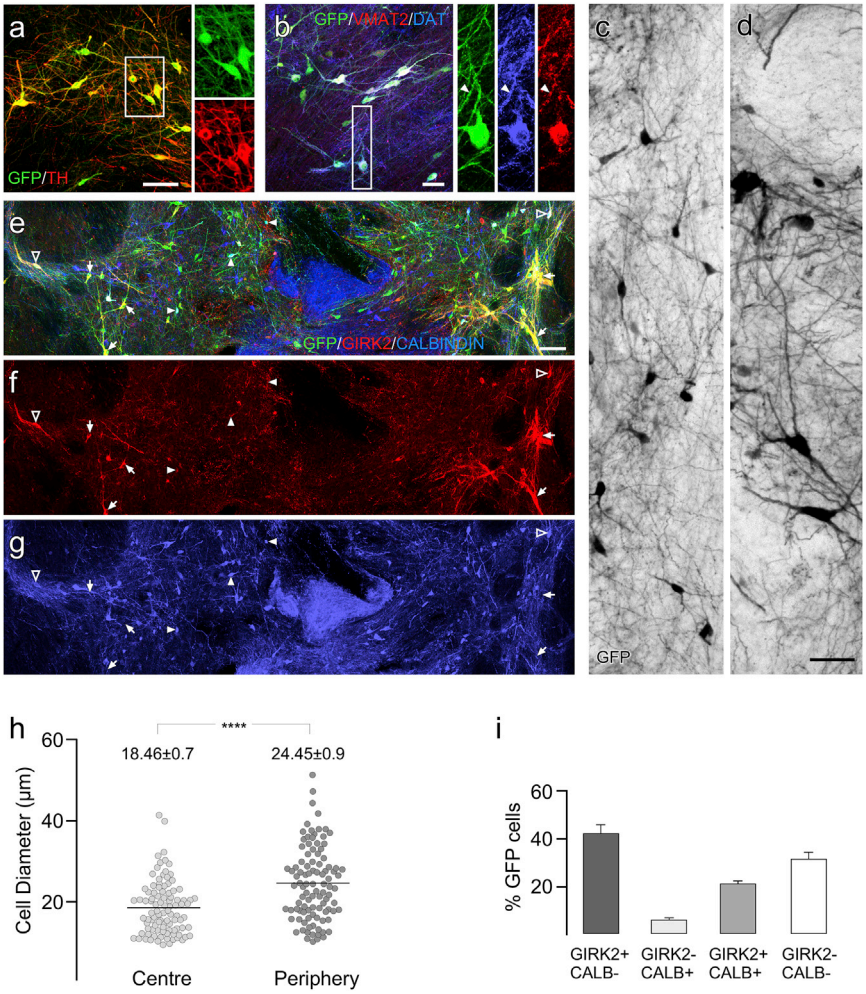

Figure 3. Immunohistochemical Identification of DA Neuronal Subtypes in Grafts at 28 Weeks

(A) The vast majority of EGFP$^+$ cells were TH$^+$ with typical midbrain dopamine neuron morphology.

(B–G) Most EGFP$^+$ DA neurons also expressed VMAT and DAT with a punctate pattern typical for these proteins (closed arrowheads). Cytoplasmic distribution of EGFP showed a mix of neuronal morphologies including smaller spherical neurons typical for A10 identity (C), as well as large, angular cell soma typical for A9 neurons (D). The GFP$^+$ neurons were also mixed based on GIRK2 and CALBINDIN expression and included EGFP$^+$/GIRK2$^+$/CALBINDIN$^-$ (E–G; arrows, particularly at the periphery of the grafts), EGFP$^+$/GIRK2$^+$/CALBINDIN$^+$ (E–G; open arrowheads), and a smaller contribution of EGFP$^+$/GIRK2$^-$/CALBINDIN$^+$ neurons (E–G; closed arrowheads).

(H) Comparison of the mean diameter (horizontal lines) of EGFP$^+$ cells in the periphery of the graft (n = 100; sampled across 3 grafts) showed these cells were significantly larger than those located more centrally (n = 100; sampled across 3 grafts, Student's t test: ****$p < 0.001$).

(I) Fractional contribution of GIRK2/CALBINDIN-expressing cell subtypes as a proportion of EGFP$^+$ cells (mean ± SEM; n = 5 grafts). CALB, CALBINDIN.

Scale bars, 100 µm (A, E–G) and 50 µm (B–D).

(Figure 6D), which was substantially more extensive then the EGFP$^+$ fiber patterns. The NCAM$^+$ labeling was particularly prominent in frontal cortical areas (Figures 6E and 6F) and, again, notably more extensive than the EGFP$^+$ fiber innervation. NCAM$^+$ fibers extended widely throughout the rostrocaudal axis of both hemispheres, predominately coursing along host white matter tracts, to innervate many structures not targeted by EGFP$^+$ DA innervation. This included discrete areas of concentrated fiber innervation indicative of target-directed growth, including the lateral septal nuclei (Figures 6D and 6G), perirhinal and entorhinal cortex (Figures 6D and 6I), basolateral amygdala (Figures 6D and 6J), periaqueductal gray, and caudal aspects of the ventral hippocampus (Figures 6D and 6L). Another notable feature was the presence of NCAM glia, which migrated extensively throughout the corpus callosum and adjacent cortical parenchyma and along the internal capsule as far caudally as the entopeduncular nucleus and cerebral peduncles (Figures 6D, 6H, and 6K).

An overlay of camera lucida-style reconstructions of immunohistochemistry for NCAM and EGFP illustrates the topographical distribution and relative density of dopaminergic and total (largely non-dopaminergic) patterns of graft-derived fiber outgrowth in the host brain (Figure 7A). Photomicrographs of the corresponding sections showed that the majority of TH$^+$ fibers in the striatum were graft-derived EGFP$^+$ origin, while in the cortex the EGFP$^+$/TH$^+$ fibers were clearly intermingled with a residual host derived EGFP$^-$/TH$^+$ fiber network (Figure 7B). Comparison of EGFP$^+$ and NCAM$^+$ fiber densities in specific host nuclei illustrated the relative contribution of DA and non-DA innervation of these areas (Figure 7C). There was no significant difference in EGFP$^+$ and NCAM$^+$ density in the dorsolateral striatum, indicating a largely dopaminergic innervation, while all other areas showed significantly greater NCAM$^+$ density and, thus, substantial contribution from non-DA neuronal subtypes.

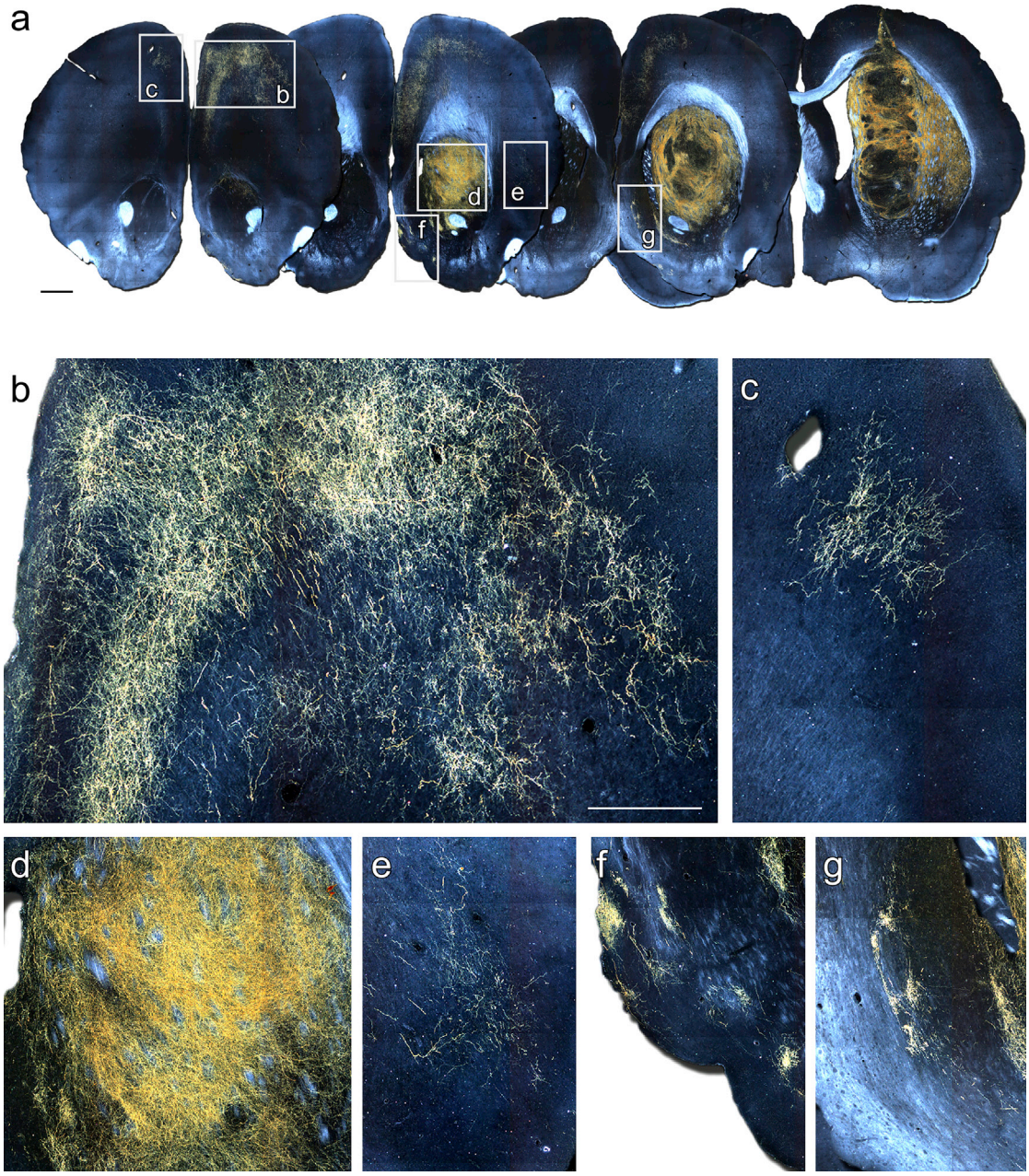

Figure 4. PITX3-eGFP Reveals Specific Patterns of Graft-Derived DA Neuron Connectivity

(A) Representative dark-field photomontages of chromogen-labeled GFP 28 weeks after grafting.

(B–G) Boxed areas from (A) are shown at higher magnification to illustrate $EGFP^+$ innervation of various host territories, including: frontal cortex ipsilateral (B) and contralateral (C) to the graft; the head of the striatum immediately rostral to the graft core (D); perirhinal cortex (E); and the islands of Calleja through the ventral palladium (F) and septum (G).

Scale bars, 1 mm (A) and 500 μm (B–G).

DISCUSSION

These results demonstrate the extent and specificity of host innervation from grafted DA neurons generated from human ESCs using contemporary differentiation and transplantation procedures. Under these conditions, *PITX3*-driven EGFP expression was highly specific for bona fide midbrain DA identity and thus allowed for precise characterization of DA-specific patterns of connectivity. The findings are similar to those from studies using fetal donor

tissue from TH-GFP or *Pitx3*-GFP reporter mice (Grealish et al., 2010; Thompson et al., 2005), showing that the grafts contain a mix of the major A9 and A10 DA neuronal subtypes and retain an intrinsic capacity to innervate multiple, developmentally appropriate host structures on a neuronal-subtype-specific basis. There were differences, however, that likely reflect species-specific aspects of midbrain cytoarchitecture and projection patterns.

The relative contribution of cell subtypes on the basis of GIRK2/CALBINDIN expression showed the predominant phenotype as GIRK2$^+$/CALBINDIN$^-$ (~47%) and only a minority as GIRK2$^-$/CALBINDIN$^+$ (~5%). This differs from grafts of fetal mouse midbrain, where there is a more marked distinction between GIRK2$^+$ and CALBINDIN$^+$ DA subtypes (Grealish et al., 2010; Thompson et al., 2005) and may represent species-specific differences in GIRK2 expression—which is broader in the human midbrain, incorporating A10 areas (Reyes et al., 2012)—but also the relatively greater ratio of A9 to A10 DA neurons in the primate brain compared to rodents (for review see Bjorklund and Dunnett, 2007). Innervation of extra-striatal territories was notably more extensive than has been reported in studies using donor tissue from reporter mice (Thompson et al., 2005), including a particularly robust innervation of frontal and cingulate cortices. Compared with rodents, the A9 DA neurons in the primate brain are known to provide a substantially greater innervation of the cortex (Bjorklund and Dunnett, 2007; Fallon and Loughlin, 1995; Lewis and Sesack, 1997). In line with this, the retrograde tracing experiments showed that while innervation of the dorsolateral striatum was overwhelmingly provided by grafted DA neurons with A9 properties, the cortex, which is predominately innervated by A10 subtypes in rodent grafting studies (Thompson et al., 2005), received innervation from both A9 and A10 subtypes. Thus overall, grafted DA neurons generated from human ESCs retain an intrinsic capacity for neuronal-subtype-specific patterns of target-directed outgrowth. These results also highlight the requirement for differentiation procedures resulting in appropriately patterned A9 neurons for establishment of terminal networks in territories relevant for restoration of motor function, including the dorsolateral striatum.

Both the time course for impact on motor function and the development of a graft-derived DA terminal network in the striatum were notably protracted. The first significant reduction in amphetamine-induced rotational asymmetry was apparent from 16 weeks and was complemented by the progressive development in density of striatal innervation between 10 and 28 weeks. This is consistent with other recent grafting studies using human embryonic stem (Kirkeby et al., 2017; Kriks et al., 2011; Niclis et al., 2017b) or induced pluripotent stem (Doi et al., 2014; Kikuchi et al., 2017) donor cells, where functional impact required 3–5 months, and also observations in PD patients receiving fetal tissue grafts, in whom clinical improvement occurs gradually between 6 and 24 months (Lindvall and Hagell, 2000). It supports the view that, irrespective of the fetal or stem cell origin of the donor material, therapeutic benefit requires that grafted midbrain DA neurons establish a functional terminal network and is unlikely to be related to indirect mechanisms, such as neuroprotection or host neuroplasticity, as has been suggested in recent studies using parthenogenetic stem cells (Gonzalez et al., 2016). Such conclusions are also supported by recent studies using light-activated opsins (Steinbeck et al., 2015) or synthetic ligand-receptor systems (Chen et al., 2016) to illustrate the relationship between correction of motor function and functional integration of implanted DA neurons.

Use of a *PITX3*-EGFP reporter line provided the unique opportunity to assess the relative contribution of host innervation from midbrain DA neurons compared with the total extent of graft-derived host connectivity. The results showed that the overwhelming majority of graft-derived outgrowth was non-dopaminergic, even in DA-specific target areas including the striatum and cortex. Non-dopaminergic axonal growth extended predominately via host white matter tracts to provide extensive innervation of remote nuclei throughout both hemispheres. In some areas, including amygdaloid nuclei, the pattern of connectivity appeared highly targeted, suggesting innervation by phenotypically specified neuronal subtypes. The overall pattern of fiber outgrowth was similar to those reported in fetal ventral mesencephalic xenografting studies (Isacson and Deacon, 1996; Thompson et al., 2008), which also include a predominately non-DA component. To some degree this may reflect developmentally appropriate outgrowth of non-DA ventral midbrain neuronal subtypes, for example GABAergic projection neurons of the substantia nigra pars reticulata, ventral tegmental area, and mammillary region that are known to project extensively to thalamus and cortex (Beckstead et al., 1979; Cornwall and Phillipson, 1988; Shibata, 1992). We identified GABA-containing cells in the stem cell-derived grafts, including those that innervated the host cortex; however, both here and in other recent studies (Doi et al., 2014; Grealish et al., 2014; Hallett et al., 2015; Kirkeby et al., 2017; Kriks et al., 2011; Samata et al., 2016), the majority of grafted neurons were not readily identified based on neurochemical features. This may indicate that many of the immature neural progenitors in the donor cell preparations are insufficiently specified to acquire a terminally differentiated phenotype after transplantation. In this case it is possible that the axonal growth trajectories will be through permissive growth corridors determined by the host environment, rather than intrinsically specified

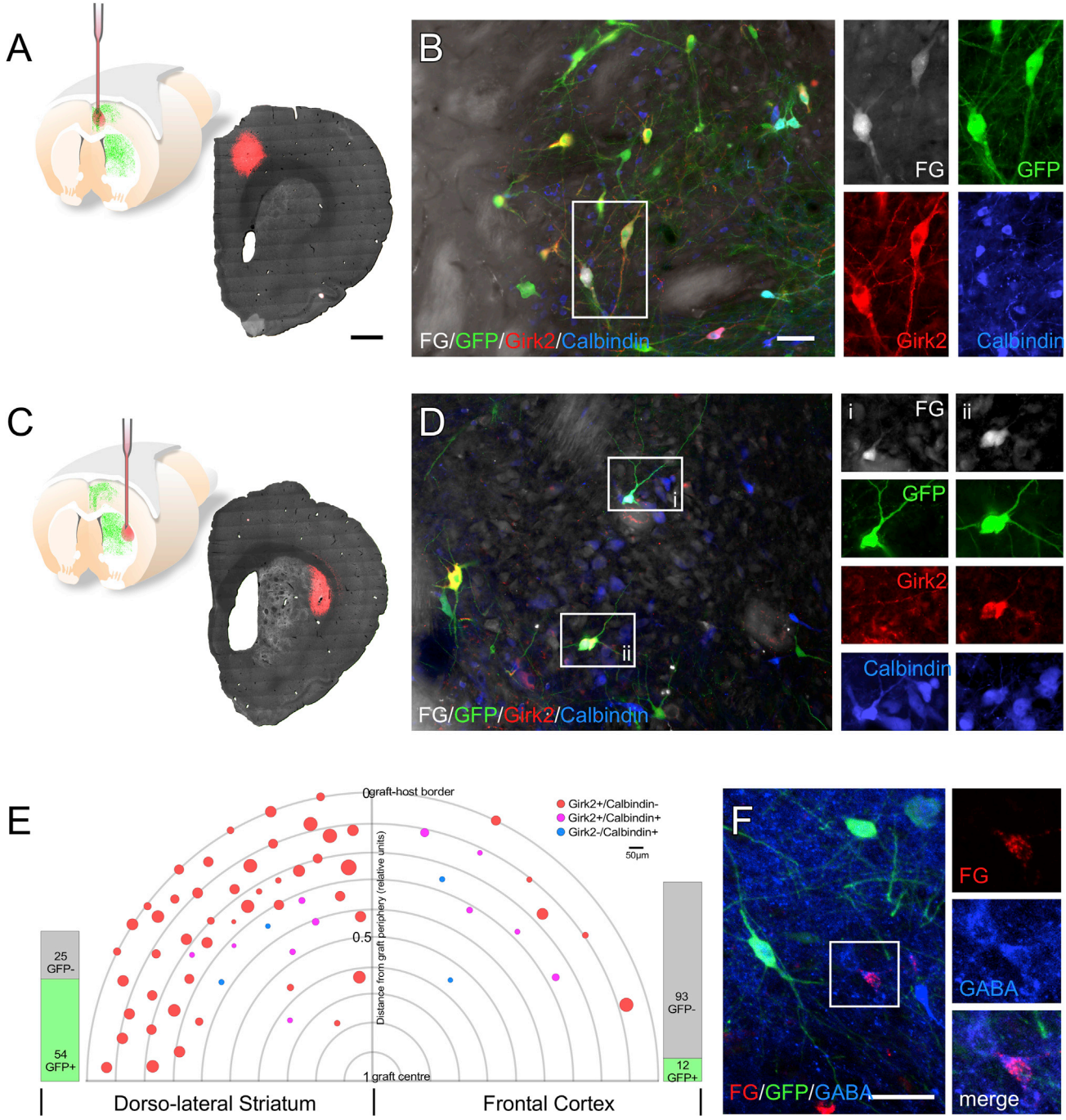

Figure 5. DA Neuronal-Subtype-Specific Innervation of Host Targets

Small deposits of Fluorogold (FG) were injected into the dorsolateral striatum (A) or frontal cortex (C) 27 weeks after grafting. The deposits were verified as being located remotely to the graft core for each animal as shown in photomontages of fluorescent detection of EGFP (grayscale; note $EGFP^+$ fiber network can be seen in the striatum) and FG (red) in representative coronal sections (A and B). Detection of FG (grayscale), EGFP (green), GIRK2 (red), and CALBINDIN (blue) in animals receiving FG in either the dorsolateral striatum (B) or frontal cortex (D) highlight representative examples of DA neuronal phenotypes projecting to these regions. A total of 79 FG^+ grafted cells were detected in animals injected with FG in the dorsolateral striatum, of which 54 were $EGFP^+$ DA neurons and a total of 105 were detected in animals injected in the frontal cortex, of which only 12 were $EGFP^+$ DA neurons (E). For each FG^+ cell the relative location on the axis between the center of the graft and the graft-host border is indicated as well as the soma size (maximum diameter) and the

(legend continued on next page)

patterns of target-directed connectivity. Consistent with such an explanation, very similar growth patterns characterized by extensive elongation along host white matter tracts has been observed also after transplantation of other donor cell identities, including cortical cell types (Denham et al., 2012b; Niclis et al., 2017a; Somaa et al., 2017). The functional consequences of non-DA connectivity remain largely unknown. While this is an area for ongoing work, it is worth noting that the similarly large contribution of non-DA neuronal outgrowth from fetal grafts has not been identified as problematic or offsetting the overall therapeutic impact provided by the DA neuronal replacement. One notable exception is the inclusion of serotonin neurons, which have been reported as a risk for graft-induced dyskinesia (Carlsson et al., 2007, 2009; Politis et al., 2010).

The average yield of DA neurons in the grafts at 28 weeks was 5,268 ± 654 per 100,000 cells implanted. This figure is consistent across a number of recent grafting studies using similar experimental designs, including reports of ~3,716 (Kirkeby et al., 2017), ~6,000 (Kriks et al., 2011), and ~8,338 (Kirkeby et al., 2012) for ESCs and ~3,436 (Doi et al., 2014) and ~8,849 (Samata et al., 2016) for iPSCs. Thus the final yield of DA neurons using currently available differentiation and transplantation techniques is in the order of 3.4%–8.8% of cells implanted. This fractional contribution may become considerably smaller with continued growth of the non-DA component over time. Here we observed that the number of DA neurons did not expand between 4 (6,081 ± 659) and 28 weeks (5,268 ± 654), while there was a significant increase in graft volume from 0.8 ± 0.28 mm^3 to 7.04 ± 0.91 mm^3 over the same time frame. We have previously reported that neural grafts derived from human PSCs exhibit ongoing cell proliferation *in vivo* as the basis for expansion of the graft volume (Denham et al., 2012b; Niclis et al., 2017a). Human fetal grafts are also known to expand *in vivo* (Labandeira-Garcia et al., 1991) and, thus, expansion of stem cell-derived grafts may represent normal developmental growth properties of human neural tissue. On current evidence, however, one cannot unambiguously exclude the possibility of slow but potentially pathological growth over clinically relevant post-transplantation time frames. This is an area that warrants further attention and various strategies are actively being pursued to safeguard against this risk, including the use of cell-sorting techniques to remove unwanted cell types (Doi et al., 2014; Gennet et al., 2016; Samata et al., 2016) or ligand-activated suicide genes to eliminate proliferating cells *in vivo* (Itakura et al., 2017; Tieng et al., 2016). A recent study by Kirkeby et al. (2017) highlights that there is also scope for ongoing refinement of differentiation procedures to optimize graft composition, with increased efficiency in specification of midbrain DA identity *in vitro* resulting in a significant increase in DA neuron density in the resulting grafts.

In summary, we report here that midbrain DA neurons generated from human ESCs establish highly specific patterns of growth *in vivo*, including innervation of developmentally appropriate targets on a DA neuronal-subtype-specific basis. The delayed onset of functional recovery and protracted course of striatal innervation by midbrain DA neurons with predominately A9 features reinforces the notion that therapeutic benefit from stem cell-based treatments for PD requires functional integration of correctly specified DA neuronal subtypes. Furthermore, the relatively small contribution of DA neurons to the overall pattern of neuronal integration highlights the scope for further refinement of current differentiation and transplantation protocols. This should include efforts to limit the inclusion of unwanted or uncharacterized cell types. The inability to standardize and characterize fetal tissue preparations prior to transplantation has been recognized as one of the key factors underlying highly variable clinical outcomes to date (Barker et al., 2015; Thompson and Bjorklund, 2012). It is therefore imperative that the same issues are avoided as enthusiasm builds for advancement of human PSCs toward clinical trials in patients with PD. Recent advances in differentiation (Kirkeby et al., 2017) and cell sorting (Doi et al., 2014; Gennet et al., 2016; Samata et al., 2016) procedures give cause for optimism.

EXPERIMENTAL PROCEDURES

Animals and Ethics

All procedures were conducted in accordance with the Australian National Health and Medical Research Council's published Code of Practice for the Use of Animals in Research, and experiments were approved by the Florey Institute of Neuroscience and Mental Health Animal Ethics Committee.

A total of 23 male athymic (CBH^{rnu}) rats at 8–9 weeks of age (~150 g) were used at the beginning of this study. The animals were group housed in individually ventilated cages with Alphadri paper bedding material (Abel Scientific, Perth) to reduce skin and eye irritation and housed on a 12:12-hr light/dark cycle with *ad libitum* access to food and water.

GIRK2/CALBINDIN expression profile. Dopamine neurons ($EGFP^+$) retrogradely labeled (FG^+) from the dorsolateral striatum are plotted on the left of the graph and $EGFP^+/FG^+$ neurons retrogradely labeled from frontal cortex are plotted on the right. A number of examples of GABA-containing neurons retrogradely labeled from cortex were also observed in the grafts (F).

Scale bars, 1 mm (A and C); 50 μm (B, D, and F). The schematic in (A) is modified from an original created by Bengt Mattsson (Lund University, Sweden).

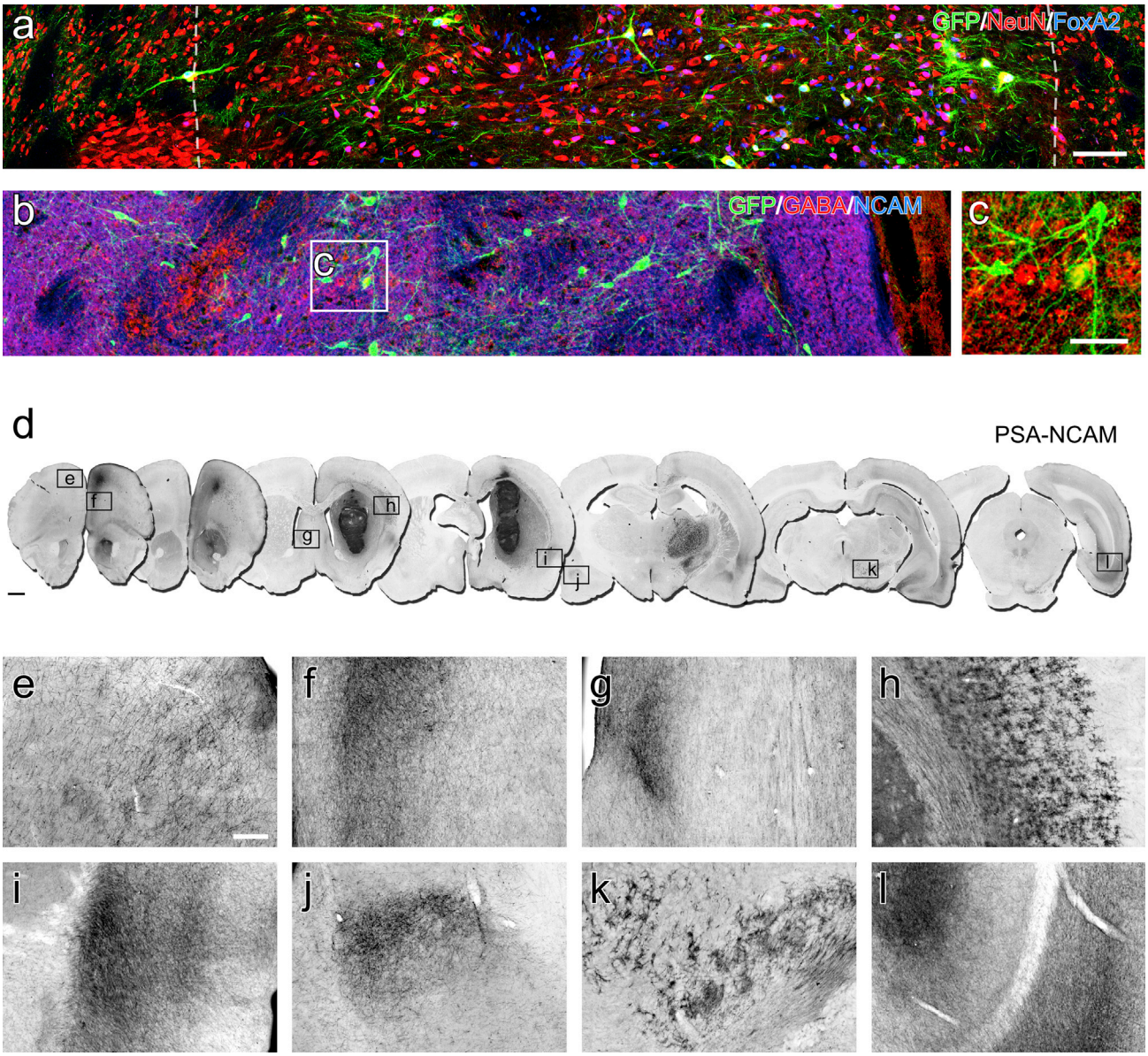

Figure 6. Grafts are Heteregenous in Composition and Contain Predominately Non-DA Neuronal Subtypes

(A) Immunohistochemistry for EGFP, NeuN, and FOXA2 at 28 weeks illustrates the relative contribution of DA neurons ($EGFP^+/NeuN^+/FOXA2^+$) and non-DA neurons ($NeuN^+/GFP^-$) as well as ventralized ($FOXA2^+$) cell types which included both neurons ($NeuN^+$) and $NeuN^-$, presumably immature, cell types (dashed lines approximate the graft-host border).

(B and C) The graft was highly immunoreactive for GABA (red), where human NCAM defines the graft (blue) and EGFP (green) is included to show DA neurons (B). Individual GABA neurons are difficult to resolve but can be delineated in the enlarged boxed area (C).

(D–L) Human-specific detection of NCAM in representative coronal sections (D) illustrates the overall extent of graft-derived fiber outgrowth, with prominent innervation of various host territories including, but not limited to: the frontal cortex contralateral (E) and ipsilateral (F) to the graft; lateral septal nuclei (G); perirhinal cortex (I); basolateral amygdala (J, contralateral hemisphere shown); and caudal aspects of the ventral hippocampus (L). Cells with glial morphology migrated extensively through host white matter tracts, particularly adjacent to the corpus callosum (H), and migrated long distances as far caudally as the midbrain (K).

Scale bars, 100 μm (A and B), 50 μm (C), 1 mm (D), 200 μm (E; applies to E–L).

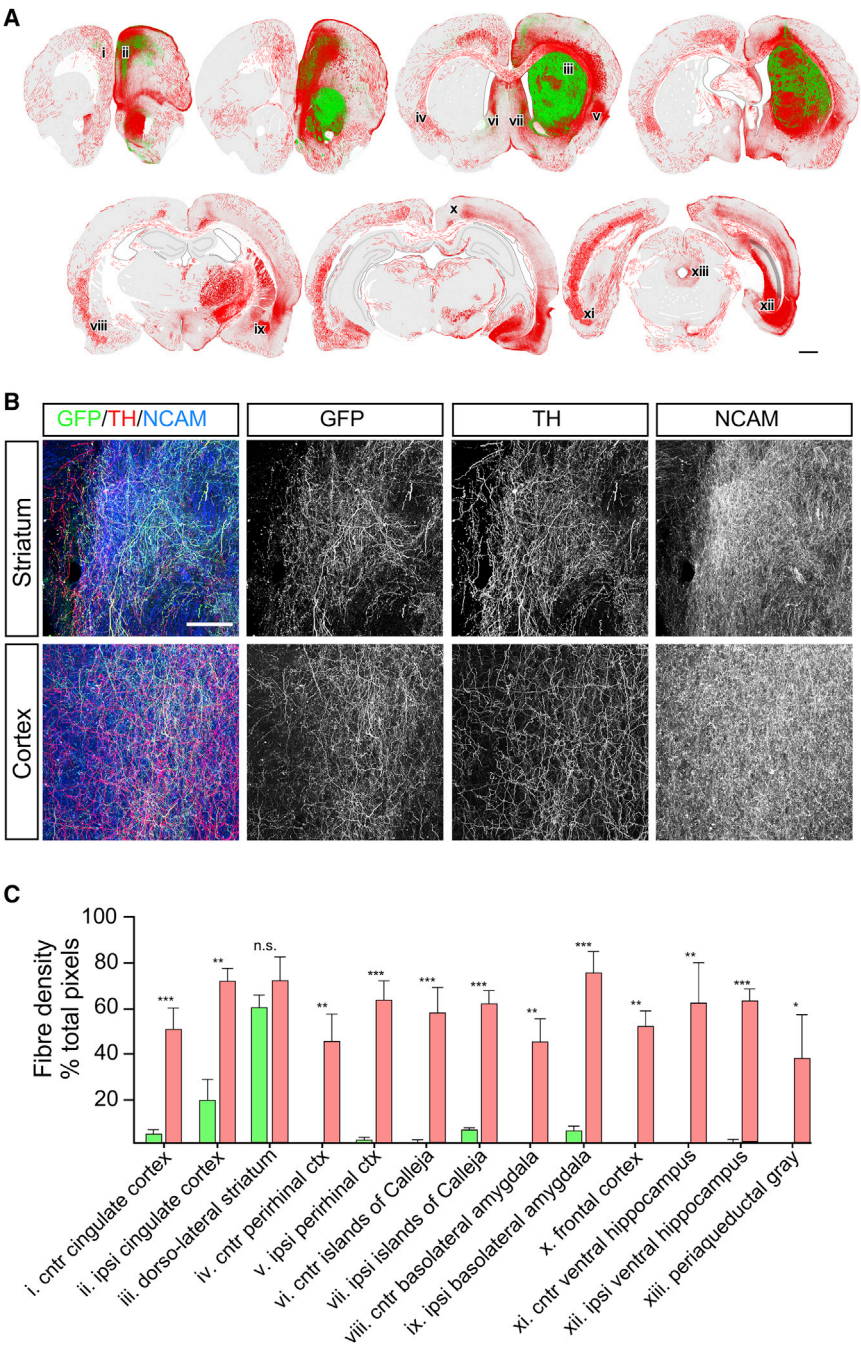

Figure 7. The Non-DA Component in ES-Derived Grafts Provides Extensive Innervation of the Host

Schematic reconstruction of immunohistochemistry for NCAM and EGFP illustrates the extent and pattern of DA-specific innervation of the host ($EGFP^+/NCAM^+$, green) relative to the total non-DA innervation ($EGFP^-/NCAM^+$, red) in a representative example 28 weeks after grafting (A). Photomicrographs from the striatum and cortex show dense fiber $EGFP^+$, TH^+, and $NCAM^+$ fiber networks and illustrate the relative contribution of $NCAM^+$ fibers as substantially greater than the graft-derived DA innervation in both areas (B). Quantification of $NCAM^+$ and $EGFP^+$ fiber density (mean ± SEM; n = 5 grafts) in specific host nuclei illustrates the relative contribution of DA and non-DA innervation in each region (C; *p < 0.05, **p < 0.01, ***p < 0.005; n.s., not significant).

Scale bars, 1 mm (A) and 100 μm (B).

Human Pluripotent Stem Cell Culture

The human embryonic stem cell *PITX3*-EGFP reporter line was generated on an H9 background as originally described (Watmuff et al., 2015) and expanded and differentiated under xeno-free conditions also as previously described in detail (Niclis et al., 2017b). In brief, neural induction was achieved via dual SMAD inhibition using LDN193189 (200 nM, days 0–11; Stemgent) and SB431542 (10 μM, days 0–5; R&D Systems). Ventral midbrain patterning was achieved by addition of sonic hedgehog (C25II, 100 ng/mL; R&D Systems), purmorphamine (2 μM, days 1–7; Stemgent), and CHIR99021 (3 μM, days 3–13; Miltenyi). At day 19, cultures rich in ventral midbrain progenitors were dissociated with Accutase (Innovative Cell Technologies) and prepared for transplantation as a cell suspension in day-19 culture medium supplemented with 0.05% DNase (Sigma).

Surgical Procedures and Rotational Behavior

Anesthesia for all surgical procedures was induced and maintained by inhaled isoflurane (2%–5% in air). All 23 athymic rats received stereotaxic injection of 3.5 μL 6-hydroxydopamine

(6-OHDA) (3.2 μg/μL free base) unilaterally into the medial forebrain bundle (3.4 mm caudal and 1.3 mm lateral to bregma and 6.8 mm below the dural surface) as previously described (Thompson et al., 2013). Three weeks later, all animals were tested for rotational asymmetry after administration of D-amphetamine sulfate (2.5 mg/kg, intraperitoneally) as described by Thompson et al. (2013). A cohort of 13 out of 23 of the animals satisfied our criteria of >7 full turns/min for designation of stable rotational asymmetry. For longitudinal assessment of rotational behavior, these animals were divided into a control group (n = 7) and a transplantation group (n = 6). The remaining 10 animals received grafts of ventral midbrain progenitors for additional histological analysis only.

One week after pre-graft rotational assessment (4 weeks after 6-OHDA) a total of 16 6-OHDA-lesioned animals received single 1-μL injections of pre-differentiated human *PITX3*-EGFP donor cells (1×10^5 cells/μL) into the rostral head of the striatum as previously described in detail (Thompson et al., 2013). Assessment of amphetamine-induced rotational behavior was performed at 8, 16, and 28 weeks after transplantation.

For retrograde labeling of grafted neurons, a Neuros syringe (Hamilton) was used to microinject 0.1 μL of a 2% solution of Fluorogold (Fluorochrome) into either the dorsolateral striatum (n = 5; 1.2 mm rostral, 3.4 mm lateral to bregma; 3.6 mm below dura) or frontal cortex (n = 5; 2.7 mm rostral, 1 mm lateral to bregma; 2 mm below dura). Tracing was performed 1 week prior to the experimental endpoint at 28 weeks.

Immunohistochemistry

For histological assessment, animals were perfusion fixed (4% paraformaldehyde) and the brains were cut on the coronal plane using a freezing microtome as previously described (Thompson et al., 2005). Four animals were taken for histological assessment 4 weeks after transplantation to confirm successful engraftment, with the remainder taken at 28 weeks (n = 10). Additionally, 2 animals were perfused at 10 and 18 weeks due to spontaneous development of skin irritations that are not uncommon with long-term housing of athymic rats. This facilitated useful, albeit qualitative information on the progressive development of DA innervation of the host striatum over time (Figure 1B).

Immunohistochemical procedures on free-floating tissue sections were as described previously in detail (Thompson et al., 2005). Primary antibodies and dilutions included: 5HT (mouse, 1:10,000, Immunostar: 20080); CALBINDIN (mouse, 1:1,000, Swant Biotech: CB300); ChAT (rabbit, 1:1,000, Millipore: AB143); DAT (rat, 1:1,000, Millipore: MAB369) FoxA2 (rabbit, 1:300, SCBT: sc-6554); GFP (chicken, 1:5,000, Abcam: AB13970); GABA (rabbit, 1:5,000, Sigma: A2052); GIRK2 (rabbit, 1:500, Alomone Labs: APC-006); NeuN (mouse, 1:200, Millipore: MAB377); dopamine-β-hydroxylase (mouse, 1:10,000, Millipore: MAB308); NCAM (mouse, 1:500, clone eric-1, SCBT: sc-106); TH (rabbit or sheep, 1:800, PelFreeze: P40101-0 or P60101-0); VMAT2 (rabbit, 1:1,000, Millipore: AB1598P). The bound primary antibody was detected either through enzymatic conjugation of the diaminobenzidine chromagen or fluorescent secondary antibodies (Jackson Immunoresearch).

Imaging and Graft Reconstructions

A Leica microscope (DM6000) with a motorized x-y stage was used to capture photomontages of whole coronal sections with chromogen-labeled EGFP or NCAM. Images were acquired either in bright field or dark field to visualize graft-derived fiber outgrowth. Photomicrographs of immunofluorescence were acquired using a Zeiss (Z780) microscope.

For analysis of cells labeled by retrograde FG uptake, cell size was recorded as the longest linear diameter for each FG^+ cell. The relative position of each FG^+ cell within the graft was calculated by determining the radial size of the graft on the dorsoventral and mediolateral axes and determining the distance from the edge of the graft along the nearest axis. To normalize for different graft sizes, the results are reported as a fractional distance along the axis where the graft periphery and center are assigned as 0 and 1, respectively.

High-resolution photomontages of whole coronal sections immunolabeled for EGFP and NCAM were used to schematically illustrate the extent and pattern of DA (EGFP) and total (NCAM) outgrowth. The "select>color-range" tool (Photoshop 13.0.6, Adobe) was initially used to define and select the bulk of the EGFP or NCAM signal. Conservative threshold levels were used to avoid selection of background signal. Each section was subsequently annotated manually by carefully tracing over the remaining fibers using a tablet-stylus interface (Intuos Pro, Wacom) and Canvas Draw software (3.0.5, ACD Systems).

Quantification and Statistics

Rotational response to amphetamine was quantified using an automated system as described by Bye et al. (2015) and group difference in mean assessed separately at each time point by Student's unpaired t test (control, n = 7; graft, n = 8 at each time point).

The mean number of EGFP cells at 4 weeks (n = 4) and 28 weeks (n = 10) was determined by counting all cells in 6 series for each animal. Double-counting error was corrected by the method of Abercrombie according to section thickness and average cell diameter (Abercrombie, 1946). The size of 200 $EGFP^+$ cells was measured as the largest linear diameter and was used to compare cell size in the periphery of the graft—defined as within 300 μm of the host-graft interface—with those located in the center. Graft volumes were calculated in the same animals by extrapolation of the cumulative area measured in 6 series using Cavalieri's principle (Cavalieri, 1966). Difference in mean volume between the 4-week (n = 4) and 28-week (n = 10) time point was assessed using Student's t test.

The overlap between TH and EGFP was determined through careful inspection of 267 $EGFP^+$ cells in confocal datasets including separate channel information on the x, y, and z axes. Similarly, the $GIRK2^+$/$CALBINDIN^+$ profile of grafted DA neurons was assessed through careful inspection of all $EGFP^+$ cells in grafts (n = 5) in single sections captured via confocal microscopy.

The relative density of graft-derived DA ($EGFP^+$/$NCAM^+$) or non-DA ($EGFP^-$/$NCAM^+$) fiber networks was assessed in specific host nuclei by measurement of $EGFP^+$ (n = 7) and $NCAM^+$ (n = 3) immunolabeled fibers as the fractional pixel contribution to single photomicrographs acquired using a 40× objective. Difference in the mean density at each location was assessed using Student's t test.

AUTHOR CONTRIBUTIONS

Conceptualization, J.C.N., C.L.P., and L.H.T.; Methodology, J.C.N., J.A.K., C.L.P., and L.H.T.; Investigation, J.C.N., C.G., C.H., J.A.K., J.D., C.L.P., and L.H.T.; Provision of Resources, J.M.H. and C.W.P.; Writing – Original Draft, J.C.N., C.L.P, and L.H.T.; Writing – Review and Editing, J.C.N., C.G., C.W.P., C.L.P., and L.H.T.; Funding Acquisition, C.L.P and L.H.T.

ACKNOWLEDGMENTS

The authors thank Mong Tien for expert technical assistance. C.P. is a Viertel Senior Research Fellow. This work was supported NHMRC project grants #1042584 and #1102704. The Florey Institute of Neuroscience and Mental Health acknowledges the strong support from the Victorian Government and in particular the funding from the Operational Infrastructure Support Grant.

Received: June 2, 2017
Revised: August 3, 2017
Accepted: August 4, 2017
Published: August 31, 2017

REFERENCES

Abercrombie, M. (1946). Estimation of nuclear population from microtome sections. Anat. Rec. *94*, 239–247.

Barker, R.A., Drouin-Ouellet, J., and Parmar, M. (2015). Cell-based therapies for Parkinson disease-past insights and future potential. Nat. Rev. Neurol. *11*, 492–503.

Beckstead, R.M., Domesick, V.B., and Nauta, W.J. (1979). Efferent connections of the substantia nigra and ventral tegmental area in the rat. Brain Res. *175*, 191–217.

Bjorklund, A., and Dunnett, S.B. (2007). Dopamine neuron systems in the brain: an update. Trends Neurosci. *30*, 194–202.

Brederlau, A., Correia, A.S., Anisimov, S.V., Elmi, M., Roybon, L., Paul, G., Morizane, A., Bergquist, F., Riebe, I., Nannmark, U., et al. (2006). Transplantation of human embryonic stem cell-derived cells to a rat model of Parkinson's disease: effect of in vitro differentiation on graft survival and teratoma formation. Stem Cells *24*, 1433.

Bye, C.R., Jonsson, M.E., Bjorklund, A., Parish, C.L., and Thompson, L.H. (2015). Transcriptome analysis reveals transmembrane targets on transplantable midbrain dopamine progenitors. Proc. Natl. Acad. Sci. USA *112*, E1946–E1955.

Carlsson, T., Carta, M., Winkler, C., Bjorklund, A., and Kirik, D. (2007). Serotonin neuron transplants exacerbate L-DOPA-induced dyskinesias in a rat model of Parkinson's disease. J. Neurosci. *27*, 8011–8022.

Carlsson, T., Carta, M., Munoz, A., Mattsson, B., Winkler, C., Kirik, D., and Bjorklund, A. (2009). Impact of grafted serotonin and dopamine neurons on development of L-DOPA-induced dyskinesias in parkinsonian rats is determined by the extent of dopamine neuron degeneration. Brain *132*, 319–335.

Cavalieri, B. (1966). Geometria Degli Indivisible (Unione Tipografico, Editrice).

Chen, Y., Xiong, M., Dong, Y., Haberman, A., Cao, J., Liu, H., Zhou, W., and Zhang, S.C. (2016). Chemical control of grafted human PSC-derived neurons in a mouse model of Parkinson's disease. Cell Stem Cell *18*, 817–826.

Cho, M.S., Lee, Y.E., Kim, J.Y., Chung, S., Cho, Y.H., Kim, D.S., Kang, S.M., Lee, H., Kim, M.H., Kim, J.H., et al. (2008). Highly efficient and large-scale generation of functional dopamine neurons from human embryonic stem cells. Proc. Natl. Acad. Sci. USA *105*, 3392–3397.

Cornwall, J., and Phillipson, O.T. (1988). Afferent projections to the dorsal thalamus of the rat as shown by retrograde lectin transport. II. The midline nuclei. Brain Res. Bull. *21*, 147–161.

Denham, M., Bye, C., Leung, J., Conley, B.J., Thompson, L.H., and Dottori, M. (2012a). Glycogen synthase kinase 3beta and activin/nodal inhibition in human embryonic stem cells induces a pre-neuroepithelial state that is required for specification to a floor plate cell lineage. Stem Cells *30*, 2400–2411.

Denham, M., Parish, C.L., Leaw, B., Wright, J., Reid, C.A., Petrou, S., Dottori, M., and Thompson, L.H. (2012b). Neurons derived from human embryonic stem cells extend long-distance axonal projections through growth along host white matter tracts after intra-cerebral transplantation. Front. Cell Neurosci. *6*, 11.

Doerr, J., Schwarz, M.K., Wiedermann, D., Leinhaas, A., Jakobs, A., Schloen, F., Schwarz, I., Diedenhofen, M., Braun, N.C., Koch, P., et al. (2017). Whole-brain 3D mapping of human neural transplant innervation. Nat. Commun. *8*, 14162.

Doi, D., Samata, B., Katsukawa, M., Kikuchi, T., Morizane, A., Ono, Y., Sekiguchi, K., Nakagawa, M., Parmar, M., and Takahashi, J. (2014). Isolation of human induced pluripotent stem cell-derived dopaminergic progenitors by cell sorting for successful transplantation. Stem Cell Reports *2*, 337–350.

Espuny-Camacho, I., Michelsen, K.A., Gall, D., Linaro, D., Hasche, A., Bonnefont, J., Bali, C., Orduz, D., Bilheu, A., Herpoel, A., et al. (2013). Pyramidal neurons derived from human pluripotent stem cells integrate efficiently into mouse brain circuits in vivo. Neuron *77*, 440–456.

Fallon, J.H., and Loughlin, S.E. (1995). Substantia nigra. In The Rat Nervous System, Second Edition, G. Paxinos, ed. (Academic Press), pp. 215–237.

Gennet, N., Tamburini, C., Nan, X., and Li, M. (2016). FolR1: a novel cell surface marker for isolating midbrain dopamine neural progenitors and nascent dopamine neurons. Sci. Rep. *6*, 32488.

Gonzalez, R., Garitaonandia, I., Poustovoitov, M., Abramihina, T., McEntire, C., Culp, B., Attwood, J., Noskov, A., Christiansen-Weber, T., Khater, M., et al. (2016). Neural stem cells derived from human parthenogenetic stem cells engraft and promote recovery in a nonhuman primate model of Parkinsons disease. Cell Transplant *25*, 1945–1966.

Grealish, S., Jonsson, M.E., Li, M., Kirik, D., Bjorklund, A., and Thompson, L.H. (2010). The A9 dopamine neuron component in grafts of ventral mesencephalon is an important determinant for recovery of motor function in a rat model of Parkinson's disease. Brain *133*, 482–495.

Grealish, S., Diguet, E., Kirkeby, A., Mattsson, B., Heuer, A., Bramoulle, Y., Van Camp, N., Perrier, A.L., Hantraye, P., Bjorklund,

A., et al. (2014). Human ESC-derived dopamine neurons show similar preclinical efficacy and potency to fetal neurons when grafted in a rat model of Parkinson's disease. Cell Stem Cell *15*, 653–665.

Hagell, P., and Brundin, P. (2001). Cell survival and clinical outcome following intrastriatal transplantation in Parkinson disease. J. Neuropathol. Exp. Neurol. *60*, 741–752.

Hallett, P.J., Deleidi, M., Astradsson, A., Smith, G.A., Cooper, O., Osborn, T.M., Sundberg, M., Moore, M.A., Perez-Torres, E., Brownell, A.L., et al. (2015). Successful function of autologous iPSC-derived dopamine neurons following transplantation in a non-human primate model of Parkinson's disease. Cell Stem Cell *16*, 269–274.

Isacson, O., and Deacon, T.W. (1996). Specific axon guidance factors persist in the adult brain as demonstrated by pig neuroblasts transplanted to the rat. Neuroscience *75*, 827–837.

Isacson, O., Deacon, T.W., Pakzaban, P., Galpern, W.R., Dinsmore, J., and Burns, L.H. (1995). Transplanted xenogeneic neural cells in neurodegenerative disease models exhibit remarkable axonal target specificity and distinct growth patterns of glial and axonal fibres. Nat. Med. *1*, 1189–1194.

Itakura, G., Kawabata, S., Ando, M., Nishiyama, Y., Sugai, K., Ozaki, M., Iida, T., Ookubo, T., Kojima, K., Kashiwagi, R., et al. (2017). Fail-safe system against potential tumorigenicity after transplantation of iPSC derivatives. Stem Cell Reports *8*, 673–684.

Kikuchi, T., Morizane, A., Doi, D., Okita, K., Nakagawa, M., Yamakado, H., Inoue, H., Takahashi, R., and Takahashi, J. (2017). Idiopathic Parkinson's disease patient-derived induced pluripotent stem cells function as midbrain dopaminergic neurons in rodent brains. J. Neurosci. Res. *95*, 1829.

Kirkeby, A., Grealish, S., Wolf, D.A., Nelander, J., Wood, J., Lundblad, M., Lindvall, O., and Parmar, M. (2012). Generation of regionally specified neural progenitors and functional neurons from human embryonic stem cells under defined conditions. Cell Rep. *1*, 703–714.

Kirkeby, A., Nolbrant, S., Tiklova, K., Heuer, A., Kee, N., Cardoso, T., Ottosson, D.R., Lelos, M.J., Rifes, P., Dunnett, S.B., et al. (2017). Predictive markers guide differentiation to improve graft outcome in clinical translation of hESC-based therapy for Parkinson's disease. Cell Stem Cell *20*, 135–148.

Kriks, S., Shim, J.W., Piao, J., Ganat, Y.M., Wakeman, D.R., Xie, Z., Carrillo-Reid, L., Auyeung, G., Antonacci, C., Buch, A., et al. (2011). Dopamine neurons derived from human ES cells efficiently engraft in animal models of Parkinson's disease. Nature *480*, 547–551.

Labandeira-Garcia, J.L., Wictorin, K., Cunningham, E.T., Jr., and Bjorklund, A. (1991). Development of intrastriatal striatal grafts and their afferent innervation from the host. Neuroscience *42*, 407–426.

Lewis, D.A., and Sesack, S.R. (1997). Dopamine systems in the primate brain. In Handbook of Chemical Neuroanatomy, F.E. Bloom, A. Bjorklund, and T. Hokfelt, eds. (Elsevier), pp. 263–375.

Lindvall, O., and Hagell, P. (2000). Clinical observations after neural transplantation in Parkinson's disease. Prog. Brain Res. *127*, 299–320.

Lu, P., Woodruff, G., Wang, Y., Graham, L., Hunt, M., Wu, D., Boehle, E., Ahmad, R., Poplawski, G., Brock, J., et al. (2014). Long-distance axonal growth from human induced pluripotent stem cells after spinal cord injury. Neuron *83*, 789–796.

Niclis, J., Gantner, C., Alsanie, W., McDougal, S., Bye, C., Elefanty, A.G., Stanley, E.G., Haynes, J., Pouton, C., Thompson, L.H., et al. (2017b). Highly efficient specification of midbrain dopamine phenotype from pluripotent stem cells under xeno-free conditions. Stem Cells Transl. Med. *6*, 937–948.

Niclis, J.C., Turner, C., Durnall, J., McDougal, S., Kauhausen, J.A., Leaw, B., Dottori, M., Parish, C.L., and Thompson, L.H. (2017a). Long-distance axonal growth and protracted functional maturation of neurons derived from human induced pluripotent stem cells after intracerebral transplantation. Stem Cells Transl. Med. *6*, 1547.

Park, C.H., Minn, Y.K., Lee, J.Y., Choi, D.H., Chang, M.Y., Shim, J.W., Ko, J.Y., Koh, H.C., Kang, M.J., Kang, J.S., et al. (2005). In vitro and in vivo analyses of human embryonic stem cell-derived dopamine neurons. J. Neurochem. *92*, 1265–1276.

Politis, M., Wu, K., Loane, C., Quinn, N.P., Brooks, D.J., Rehncrona, S., Bjorklund, A., Lindvall, O., and Piccini, P. (2010). Serotonergic neurons mediate dyskinesia side effects in Parkinson's patients with neural transplants. Sci. Transl. Med. *2*, 38ra46.

Qi, Y., Zhang, X.J., Renier, N., Wu, Z., Atkin, T., Sun, Z., Ozair, M.Z., Tchieu, J., Zimmer, B., Fattahi, F., et al. (2017). Combined small-molecule inhibition accelerates the derivation of functional cortical neurons from human pluripotent stem cells. Nat. Biotechnol. *35*, 154–163.

Reyes, S., Fu, Y., Double, K., Thompson, L., Kirik, D., Paxinos, G., and Halliday, G.M. (2012). GIRK2 expression in dopamine neurons of the substantia nigra and ventral tegmental area. J. Comp. Neurol. *520*, 2591.

Samata, B., Doi, D., Nishimura, K., Kikuchi, T., Watanabe, A., Sakamoto, Y., Kakuta, J., Ono, Y., and Takahashi, J. (2016). Purification of functional human ES and iPSC-derived midbrain dopaminergic progenitors using LRTM1. Nat. Commun. *7*, 13097.

Sawamoto, K., Nakao, N., Kobayashi, K., Matsushita, N., Takahashi, H., Kakishita, K., Yamamoto, A., Yoshizaki, T., Terashima, T., Murakami, F., et al. (2001). Visualization, direct isolation, and transplantation of midbrain dopaminergic neurons. Proc. Natl. Acad. Sci. USA *98*, 6423–6428.

Shibata, H. (1992). Topographic organization of subcortical projections to the anterior thalamic nuclei in the rat. J. Comp. Neurol. *323*, 117–127.

Somaa, F.A., Wang, T.Y., Niclis, J.C., Bruggeman, K.F., Kauhausen, J.A., Guo, H., McDougall, S., Williams, R.J., Nisbet, D.R., Thompson, L.H., and Parish, C.L. (2017). Peptide-based scaffolds support human cortical progenitor graft integration to reduce atrophy and promote functional repair in a model of stroke. Cell Reports *20*, 1964–1977.

Sonntag, K.C., Pruszak, J., Yoshizaki, T., van Arensbergen, J., Sanchez-Pernaute, R., and Isacson, O. (2007). Enhanced yield of neuroepithelial precursors and midbrain-like dopaminergic neurons from human embryonic stem cells using the bone morphogenic protein antagonist noggin. Stem Cells *25*, 411–418.

Steinbeck, J.A., Choi, S.J., Mrejeru, A., Ganat, Y., Deisseroth, K., Sulzer, D., Mosharov, E.V., and Studer, L. (2015). Optogenetics enables functional analysis of human embryonic stem cell-derived grafts in a Parkinson's disease model. Nat. Biotechnol. *33*, 204–209.

Steinbeck, J.A., Koch, P., Derouiche, A., and Brustle, O. (2012). Human embryonic stem cell-derived neurons establish region-specific, long-range projections in the adult brain. Cell. Mol. Life Sci. *69*, 461–470.

Sundberg, M., Bogetofte, H., Lawson, T., Jansson, J., Smith, G., Astradsson, A., Moore, M., Osborn, T., Cooper, O., Spealman, R., et al. (2013). Improved cell therapy protocols for Parkinson's disease based on differentiation efficiency and safety of hESC-, hiPSC-, and non-human primate iPSC-derived dopaminergic neurons. Stem Cells *31*, 1548–1562.

Thompson, L., Barraud, P., Andersson, E., Kirik, D., and Bjorklund, A. (2005). Identification of dopaminergic neurons of nigral and ventral tegmental area subtypes in grafts of fetal ventral mesencephalon based on cell morphology, protein expression, and efferent projections. J. Neurosci. *25*, 6467–6477.

Thompson, L.H., and Bjorklund, A. (2009). Transgenic reporter mice as tools for studies of transplantability and connectivity of dopamine neuron precursors in fetal tissue grafts. In Neurotherapy: Progress in Restorative Neuroscience and Neurology, J. Verhaagen, E.M. Hol, I. Huitenga, J. Wijnholds, A.B. Bergen, G.J. Boer, and D.F. Swaab, eds. (Elsevier), pp. 53–79.

Thompson, L., and Bjorklund, A. (2012). Survival, differentiation, and connectivity of ventral mesencephalic dopamine neurons following transplantation. Prog. Brain Res. *200*, 61–95.

Thompson, L.H., Kirik, D., and Bjorklund, A. (2008). Non-dopaminergic neurons in ventral mesencephalic transplants make widespread axonal connections in the host brain. Exp. Neurol. *213*, 220–228.

Thompson, L.H., Parish, C.L., Reynolds, B., and Deleyrolle, L. (2013). Transplantation of fetal midbrain dopamine progenitors into a rodent model of Parkinson's disease. Methods Mol. Biol. *1059*, 169–180.

Tieng, V., Cherpin, O., Gutzwiller, E., Zambon, A.C., Delgado, C., Salmon, P., Dubois-Dauphin, M., and Krause, K.H. (2016). Elimination of proliferating cells from CNS grafts using a Ki67 promoter-driven thymidine kinase. Mol. Ther. Methods Clin. Dev. *6*, 16069.

Watmuff, B., Hartley, B.J., Hunt, C.P., Fabb, S.A., Pouton, C.W., and Haynes, J.M. (2015). Human pluripotent stem cell derived midbrain PITX3(EGFP/w) neurons: a versatile tool for pharmacological screening and neurodegenerative modeling. Front. Cell Neurosci. *9*, 104.

Wictorin, K., Brundin, P., Sauer, H., Lindvall, O., and Bjorklund, A. (1992). Long distance directed axonal growth from human dopaminergic mesencephalic neuroblasts implanted along the nigrostriatal pathway in 6-hydroxydopamine lesioned adult rats. J. Comp. Neurol. *323*, 475–494.

Yang, D., Zhang, Z.J., Oldenburg, M., Ayala, M., and Zhang, S.C. (2008). Human embryonic stem cell-derived dopaminergic neurons reverse functional deficit in parkinsonian rats. Stem Cells *26*, 55–63.

Zhao, S., Maxwell, S., Jimenez-Beristain, A., Vives, J., Kuehner, E., Zhao, J., O'Brien, C., de Felipe, C., Semina, E., and Li, M. (2004). Generation of embryonic stem cells and transgenic mice expressing green fluorescence protein in midbrain dopaminergic neurons. Eur. J. Neurosci. *19*, 1133–1140.